Overview of transition prediction tools in the elsA software

Jean Perraud, Hugues Deniau, Grégoire Casalis

11th World Congress on Computational Mechanics (WCCM XI)
5th European Conference on Computational Mechanics (ECCM V)
6th European Conference on Computational Fluid Dynamics (ECFD VI)
July 20–25, 2014, Barcelona, Spain

OVERVIEW OF TRANSITION PREDICTION TOOLS IN THE ELSA SOFTWARE

Jean Perraud[1], Hugues Deniau[2] and Grégoire Casalis[3]

[1] ONERA - the French Aerospace lab F-31055 Toulouse, France, Jean.Perraud@onera.fr [2] ONERA, F-31055 Toulouse, France, Hugues.Deniau@onera.fr [3] ONERA, F-31055 Toulouse, France, Grégoire.Casalis@onera.fr

Key words: *Transition prediction, RANS code, elsA, Transition criteria and transport equations.*

1 Introduction

Laminar-turbulent transition has an impact on wall friction and heating, so it constitutes an important issue when a precise evaluation of friction drag or wall heating is desired. It may happen along several paths to turbulence [1] depending on the flow quality and wall nature. In case of low external turbulence flow over a smooth wall, natural transition is expected, which occurs through the growth of instabilities. This is typically the case for transport aircraft, assuming smooth surfaces. When the external turbulence level increases above about 1%, or in presence of surface roughness, a different type of amplification, linked to the forced response of the boundary layer, may cause a more rapid occurence of transition, called bypass transition.

Long term involvement of ONERA in laminar-turbulent transition modelling [2],[3],[4] and into the development of the elsA software [5],[6], with major contributions from D. Arnal, R. Houdeville et al.[7] have lead to a wealth of transition criteria and related tools in the elsA software, routinely used for wing design and quite well adapted for performance prediction. Nevertheless, transition prediction is a difficult task and the prospect of laminar wing design on one hand, and, on the other hand the ever improved design of rotating devices, from high speed propellers to turbine blades, put a renewed pressure for reliability and precision, while the current demand for ever more complex configurations calls for robustness and simplification of the use of the elsA solver regarding transition prediction.

Presently, two categories of tools coexist in elsA. First, a quite large number of transition criteria, which generally rely on boundary layer integral parameters and may (or not) take into account the boundary layer history and will be presented in section 2. Most

important among these, the so-called AHD [8] and C1 criteria [9],[10], the first one being based on systematic stability calculations of similar Falkner Skan profiles, and the second being one of the few correlations dedicated to crossflow prediction. Another criterion developped at about the same period, the Gleyzes criterion [11], looks at short bubble transition in 2D low speed flows. This first series relies in elsA on the concept of transition computation line, to be defined by the user, and along which regions are specified to be laminar, turbulent, or to be computed.

Second, the approach proposed by Menter & Langtry [12],[13],[14] based on two transport equations for an intermittency γ and a transition Reynolds number $\overline{R_{\theta_T}}$ is also available in elsA, using a closure developped by C. Content [15]. While the transition criterion contained in this approach is rather crude, the ease of application and the fairly good results which may be obtained on turbine blades [16] have made this approach a popular one, at least for given classes of applications.
The above mentioned drivers, reliability, precision, robustness and simplicity, are motivating new developments in several directions:
- Extension of the existing tools in order to model a wider range of conditions. The longitudinal criterion is being extended to higher Mach numbers, as will be presented.
- As a preliminary phase for the next step, work has started on the development of a new method, with the ideas of using transport equations as a mean to follow approximately streamlines and discard the user defined transition lines, and, at the same time, keeping the use of high fidelity criteria.
The objective is not a strictly local approach, but one that will improve the treatment of complex configurations while being compatible with the use of stability based methods. Future developments will deal with the introduction of stability based methods to replace transition criteria and improve the first two drivers, especially concerning 3D configurations and crossflow predictions. The so-called 3D Parabola method, presently available in the 3D boundary layer code $3C3D$ [17], is seen as candidate. Impact of elsA numerical options, and improved ways of coupling the method with RANS quantities will be explored in a starting Ph. D. work.

2 Criteria based transition prediction in elsA

The laminar or turbulent state of a boundary layer may be characterized using the intermittency function γ, which represents the fraction of time over which the flow is turbulent. When using transition criteria, γ is defined at wall points and its value applies to all the points along a normal to the wall direction, up to a maximal distance. γ is then used as a weighting function applied to the eddy viscosity coefficient: $\mu_{eff} = \mu + \gamma\mu_t$ In case of transport equation turbulence models for which the k production term is proportional to μ_t, using $\gamma\mu_t$ prevents the production of turbulence. A quite large number of transition criteria are available in elsA, grouped in two families, local and non-local criteria. A transition criterion is said local if only function of information defined along a normal to the wall at a given point.
Criteria which are only functions of turbulence level, some integral thicknesses and the

local pressure gradient are thus local. The pressure gradient may be expressed using the Pohlhausen parameter :

$$\Lambda_2 = \frac{\theta^2}{\nu}\frac{\mathrm{d}|\boldsymbol{U_e}|}{\mathrm{d}s}, \tag{1}$$

where θ is the momentum tickness, s is the curvilinear coordinate along the streamline at the edge of the boundary layer and $|\boldsymbol{U_e}|$ is the velocity modulus also taken at the edge of the boundary layer. In practice, using the pressure gradient at the wall is usually preferred because more readily defined in a Navier Stokes code, and more precise:

$$\Lambda_2 = -\frac{\theta^2}{\rho|\boldsymbol{U_e}|\nu}\frac{\partial p_{wall}}{\partial s} \tag{2}$$

Available criteria in elsA, deduced from experimental results, are those of Dunhamn [18], Seyb [19], Abu-Ghannam & Shaw [20], Drela [21] and Mayle [22]. These criteria were selected during the AG43 GARTEUR Project. In the following, Tu is expressed in %

A purely bypass criterion is given by Mayle, only function of Tu:

$$R_{\theta_T} = 400(Tu)^{-5/8} \tag{3}$$

Dunham criterion writes $(0.1 < Tu < 4)$:

$$R_{\theta_T} = [0.27 + 0.73\exp(-0.8Tu)][550 + \frac{680}{1 + Tu - 21\,\Lambda_{2T}}] \tag{4}$$

Seyb $(0.1 < Tu < 4)$:

$$R_{\theta_T} = \frac{1000}{1.2 + 0.7\,Tu} + 10[\frac{0.09 + \Lambda_{2T}}{0.0106 + 0.036\,Tu}]^{2.62} \tag{5}$$

Abu-Ghannam & Shaw $(0.1 < Tu < 9)$:

$$R_{\theta_T} = 163 + exp[F_\lambda(\Lambda_{2T}) - \frac{F_\lambda(\Lambda_{2T})Tu}{6.91}] \tag{6}$$

with

$$F_\lambda(\Lambda_2) = 6.91 + 12.75\Lambda_2 + 63.64{\Lambda_2}^2 \quad if \quad \Lambda_2 < 0 \tag{7}$$

$$F_\lambda(\Lambda_2) = 6.91 + 2.48\Lambda_2 - 12.27{\Lambda_2}^2 \quad if \quad \Lambda_2 > 0 \tag{8}$$

Drela's criterion is a modified version of Abu-Ghannam & Shaw, expressed using the local, incompressible shape factor $Hi = \delta_1/\theta$. This shape factor is strongly related to the longitudinal stability characteristics of the boundary layer, but its estimation in a Navier Stokes codes often lacks precision, being dependent on the determination of the boundary layer edge, and on the choice of spatial scheme and numerical dissipation. In elsA, for

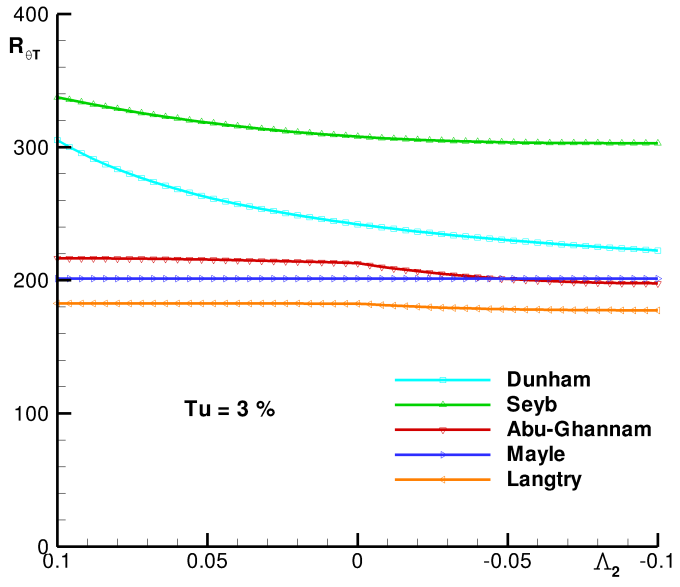

Figure 1: Transition correlations for Tu = 3.%

incompressible flow, the shape factor is estimated as a function of the local Pohlhausen parameter :

$$Hi = 4.02923 - \sqrt{-8838.4\Lambda_2^4 + 1105.1\Lambda_2^3 - 67.962\Lambda_2^2 + 17.574\Lambda_2 + 2.0593} \qquad (9)$$

It is necessary to limit Λ_2 between -0.068253 and 0.1. The lower limit corresponds to $Hi = 4$. Note that separation occurs at $Hi = 4.023$ for the Falkner-Skan solution, and in practice occurs at even lower values of Hi in Navier Stokes calculations. In compressible flows, a more complex relation can be established.
Another correlation derived from Abu-Ghannam is due to Langtry [14] and is presented in the next section. Figure 1 presents a comparison of these correlations, for Tu = 3%, represented with negative (favorable) pressure gradients on the left and positive on the right. Seyb and Dunham are quite above Abu-Ghannam and Langtry criterion. Mayle, independant of the pressure gradient, is also represented, and is quite close to Abu-Ghannam. All these criteria are expressed independently of the local Mach number, although part of the data base comes from transonic tests. Their use is mostly recommanded in case of large values of the turbulence level, i.e. bypass transition.
A local criterion dedicated to crossflow, called C1, is due to Coustols & Arnal [9],[10], and is also empirical, but contains a compressility correction. Crossflow transition is predicted when the Reynolds number R_{δ_2} becomes larger than $R_{\delta_2 T}$:

$$\begin{aligned} R_{\delta_2 T} &= 150 && if \quad Hi \leq 2.31 \\ R_{\delta_2 T} &= \frac{300}{\pi} \arctan\left(\frac{0.106}{(Hi-2.3)^{2.092}}\right)\left(1+\frac{\gamma-1}{2}M_e^2\right) && if \quad Hi > 2.31 \end{aligned} \qquad (10)$$

where $\delta_2 = \int_0^\delta \frac{w}{u_e}\, dy$ and M_e is the local Mach number. C1 should not be activated when

the shape factor grows above 2.6, as the model then produces low values of $R_{\delta_2 T}$, resulting in possible incorrect crossflow predictions in regions with positive or zero pressure gradient where crossflow is not expected. Note also that this criterion is independent of the turbulence level. This may be acceptable for flight conditions, where the initial amplitude of the stationnary vortices may be linked to the attachment line properties, but constitute a limitation when looking at wind tunnel conditions where the turbulence level has an impact on the boundary layer receptivity. The C1 criterion may be applied to swept wings where crossflow may cause transition in the first 10% chord. Other situations require special attention, see section 4.3.

Non local criteria are also available. They are those based on systematic stability calculations for similar profiles. Looking at longitudinal transition, usually caused by Tollmien-Schlichting instabilities in 2D flows, The AHD criterion (Arnal-Habiballah-Delcourt) [8] was derived from N-factor curves computed for Falkner Skan self attached similar velocity profiles. These curves are expressed as

$$N = N\left(R_\theta - R_{\theta cr}, \Lambda_2\right) \tag{11}$$

where $R_{\theta cr}$ is the critical Reynold number (where the first instabilities start to grow). The use of the Mack relationship ($N_T = -2.4\ln(Tu/100) - 8.43$) allows to express R_{θ_T} as a function of Tu and the pressure gradient. The final criterion is based on the averaged Pohlhausen parameter, this average being computed from the critical point to the current one.

$$\overline{\Lambda_2} = \frac{1}{s - s_{cr}} \int_{s_{cr}}^{s} \frac{\theta^2}{\nu} \frac{du_e}{ds}\, ds = \frac{1}{s - s_{cr}} \int_{s_{cr}}^{s} \Lambda_2 ds \tag{12}$$

The criterion itself writes :

$$R_{\theta_T} - R_{\theta_{cr}} = -206\, \exp\left(25.7\overline{\Lambda_2}_T\right)\, \left[\ln\left(16.8Tu/100.\right) - 2.77\overline{\Lambda_2}_T\right] \tag{13}$$

This criterion is activated after the detection of the critical location, identified by $R_\theta = R_{\theta_{cr}}$ where $R_{\theta_{cr}} = exp[52/Hi - 14.8]$. The formulation given here was developped for incompressible flow. The criterion has been extended to compressible flows, first up to Mach 1.6 [23] and recently up to Mach 4. In that case, equation 13 takes the form

$$R_{\theta_T} - R_{\theta_{cr}} = A \exp\left(B\overline{\Lambda_2}_T\right)\, \left[\ln\left(CTu\right) - D\overline{\Lambda_2}_T\right] \tag{14}$$

where A, B, C, D are now expressed as functions of the local Mach number Me.
In case of short bubble transition, the Gleyzes criterion [11] is also a non local criterion, based on stability calculations for 2D detached self similar velocity profiles. The criterion expresses the N-factor growth as a function of the shape factor

$$N(s) = \int_{R_{\theta\ crit}}^{R_\theta} \frac{-2.4}{B}\, \mathrm{d}R_\theta \tag{15}$$

with :

$$R_{\theta\ crit} = 1.4445 \exp\left(\frac{52}{Hi} - 14.8\right)\left[1 + \left(3.9\left|Hi - 2.56\right|\right)^{1.9}\right] \tag{16}$$

and

$$B = \begin{cases} \dfrac{-162.11093}{Hi^{1.1}} & if \quad 3.36 < Hi \\ -73\exp\left[-1.56486\left(Hi-3.02\right)\right] & if \quad 2.8 < Hi < 3.36 \\ -103\exp\left[-4.12633\left(Hi-2.8\right)\right] & if \quad Hi < 2.8 \end{cases} \tag{17}$$

The value of the transition N-factor N_T is again determined using Mack relationship $N_T = -2.4\ln(Tu/100) - 8.43$.
The Gleyzes criterion has been combined with AHD, thanks to J. Cliquet [24] in order to cover the full range of pressure gradients. To do this, a limit value Hi_{switch} is defined, equal to 2.8. The AHD criterion is used below Hi_{switch}. If Hi becomes larger than the limit, the Gleyzes criterion is used from that point on, with

$$N(s) = N_{switch} + \int_{R_{\theta_{switch}}}^{R_\theta} \frac{-2.4}{B}\,\mathrm{d}R_\theta \tag{18}$$

with B as before, and N_{switch} representing the amplification reached at the point where $Hi = Hi_{switch}$. N_{switch} is defined from Tu_{switch}, where Tu_{switch} is obtained as a function of $(R_\theta - R_{\theta_{cr}})$ by inverting eq. 13

Non local criteria in elsA are evaluated along transition lines. These lines, which should be oriented in the flow direction, are to be defined by the user and allow to impose laminar or turbulent regions, and to define where the criteria are to be considered. Several criteria may be activated in parallel. While the transition line concept is very handy, the definition of these lines by the user may become cumbersome, in case of complex configurations. It requires, for example, to have located the attachment line, especially for swept wings with fast growing instabilities. Also, the existing lines are not compatible with the chimera method.

Figure 2 gives a comparison of AHD and the previous empirical criteria as a function of Λ_2 for $Tu = 0.1\%$. AHD is defined over a smaller range of Λ_2 values, but shows a much larger dependance with the pressure gradient than the purely empirical models. A similar dependance is visible in case of Dunham and Seyb criteria, while Abu-Ghannam & Shaw and Langtry show limited variations. This may seem acceptable in case of favorable gradients, as other instabilities could become more important than the strictly longitudinal ones considered in the AHD model at Mach 0. In case of unfavorable gradients, on the other side, it seems like R_{θ_T} from the correlations is generally overestimated.
Another point of interest is the compressibility effect. From the existing database which was used to create the compressible extension to AHD, a simple model was created in order to compare the Langtry correlation to stability based variations. To this order, the expression $R_{\theta_T} - R_{\theta cr} = f(Me, Tu, \Lambda_2)$ was re-expressed in a form $R_{\theta_T} = f1(Me, Tu, \Lambda_2)$ This simple model is based on stability calculation for Falkner Skan similar profils between Mach 0 and 1.1, and is representing natural transition, for $Tu \leq 1\%$. The evolution of R_{θ_T} as a function of turbulence level, Mach number and pressure gradient is:

$$R_{\theta_T} = -(177Me^2 - 22Me + 210)ln((7Me + 4.8)Tu/100)exp((5Me + 27)\Lambda_2) \tag{19}$$

It is compared to Langtry's correlation in figure 3, while the Mach number dependance appears in figure 4. Looking at fig. 3, a good agreement with Langtry may be seen at

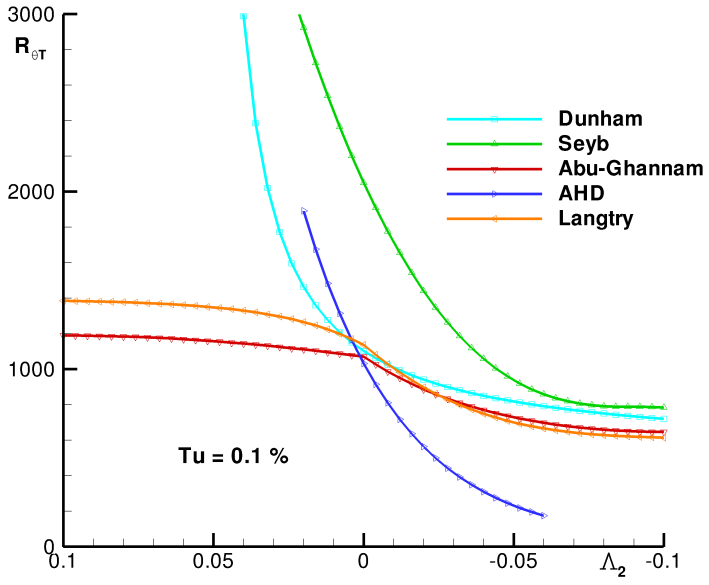

Figure 2: Transition correlations for Tu = 0.1%

$\Lambda_2 = 0$ for several values of Tu. Again, pressure gradient effects seem to be underestimated by Langtry's correlation. Note that AHD only considers attached boundary layers while the lowest values of Λ_2 in Langtry's model correspond to separated flows. This comparison is limited to the range of Tu corresponding to natural transition. Between 1 and 3%, transient growth gradually becomes the main path to turbulence, and there is little interest to compare R_{θ_T} to stability. The effect of compressibility, not taken into account in Langtry's model, is shown in figure 4 for a zero pressure gradient. R_{θ_T} increases from about 1200 at low speed to 2000 at Mach 1.1, for $Tu = 0.05\%$.

Another transition mechanism which is inherently non local is attachment line contamination, often called Attachment Line Transition (ALT). It is caused by the propagation along a swept wing leading edge of the fuselage turbulence, and is characterized by a Reynolds number $\overline{R}$. When this contamination occurs, the whole wing becomes turbulent, with no laminar region. ALT prediction requires to locate a leading edge point with respect to the wing root. A second family of lines, contamination lines, have been defined in elsA, which propagate this information. $\overline{R}$ is then evaluated and contamination predicted. The current criterion looks at contamination, occuring at $\overline{R} = 250$, but ignore transition cause by Görtler-Hammerlin instabilities, occuring at even larger values of $\overline{R}$, around 600. On a 3D wing with φ deg. sweep, $\overline{R}$ is expressed as

$$\overline{R} = \frac{W_e}{\sqrt{\nu_e k}} \quad \text{where} \quad k = \left[\frac{\partial U_e}{\partial X}\right]_{X=0} \tag{20}$$

with W_e the spanwise velocity component and U_e the velocity normal to the attachment line. For a circular cylinder of radius r, with Q_e the modulus of the velocity at the boundary layer edge, $\overline{R}$ may be shown to take the form

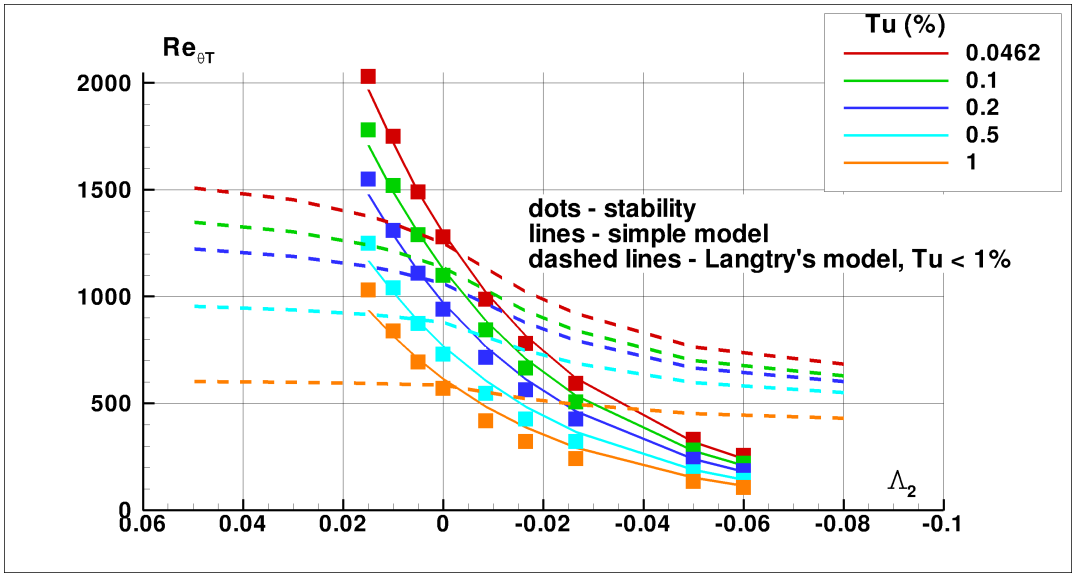

Figure 3: Comparison of a stability based model with Langtry's correlation

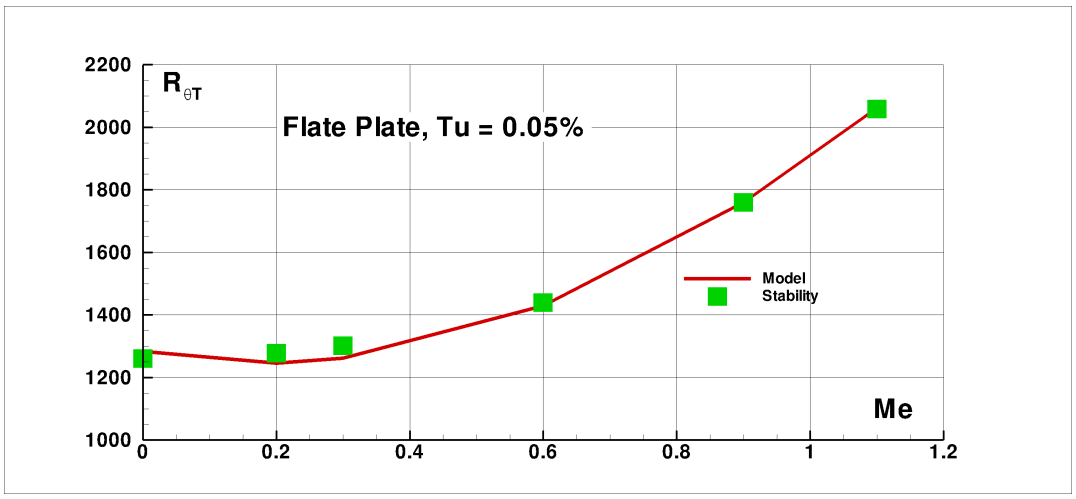

Figure 4: R_{θ_T} Mach number dependance at zero pressure gradient

$$\overline{R} = \sqrt{\frac{Q_e\, r\, sin(\varphi) tan(\varphi)}{2\nu}} \tag{21}$$

it is proportional to the square root of the Reynolds number or of the leading edge radius.

In elsA, the velocity gradient $k = \left[\frac{\partial U_e}{\partial X}\right]_{X=0}$ is obtained from the pressure gradient in the leading edge region,

$$k = \frac{|\mathbf{grad} p.X|}{\rho_e |U_{eN}|} \tag{22}$$

Because the precise direction is not know, it is assumed that the direction making $|\mathbf{grad} p.X|$ maximum will correspond to the desired direction. Also, both the gradient and $|U_{eN}|$ must be evaluated at a distance from the attachment line as they both go to zero on this line. The contamination criterion has not been made compatible with parallel processing. An example will later be presented.

3 Transport equation formulation following Menter's model

This model is based on two transport equations, one for an intermittency function γ and one for a Reynold number $\overline{R_{\theta_T}}$. Note that γ here is not the physical intermittency, but becomes a field controlling the laminar or turbulent nature of the boundary layer, while $\overline{R_{\theta_T}}$ is linked to a transition criterion, and determines the transition location. $\overline{R_{\theta_T}}$ is initialized using the Langtry's transition correlation outside the boundary layer, function of the local turbulence level and the pressure gradient. The production term in the turbulence model is then multiplied by γ, controlling the turbulent kinetic energy rise from the model.

$$\frac{\partial \rho\gamma}{\partial t} + \frac{\partial \rho U_j \gamma}{\partial x_j} = P_\gamma - E_\gamma + \frac{\partial}{\partial x_j}\left[\left(\mu + \frac{\mu_t}{\sigma_f}\right)\frac{\partial \gamma}{\partial x_j}\right] \tag{23}$$

$$\frac{\partial \rho\overline{R_{\theta_T}}}{\partial t} + \frac{\partial \rho U_j \overline{R_{\theta_T}}}{\partial x_j} = P_{\theta_T} + \frac{\partial}{\partial x_j}\left[\sigma_{\theta_T}\left(\mu + \mu_t\right)\frac{\partial \overline{R_{\theta_T}}}{\partial x_j}\right] \tag{24}$$

P_γ represents the intermittency production term, defined as :

$$P_\gamma = F_{length}\, c_{a1}\, \rho\, S\, \left(\gamma F_{onset}\right)^{0.5} \left(1 - c_{e1}\, \gamma\right), \tag{25}$$

where two functions, F_{onset} and F_{length} control the activity and the amplitude of the production. F_{onset} is related to a ratio $\frac{Re_v}{2.193\, R_{\theta_c}}$, where $Re_v = \frac{\rho y^2 \Omega}{\mu}$ represents the vorticity Reynolds number introduced by van Driest and Blumer [25] for the laminar boundary layer. Production is set to zero when the ratio remains below one. F_{length} controls the rate of production and thus the length of the transition region. Both R_{θ_c} and F_{length} functions are expressed as functions of $\overline{R_{\theta_T}}$.
Due to C. Content, the following correlation functions have been defined :

$$F_{length} = \max\left[10^{-4}; exp(-1.32510^{-8}\overline{R_{\theta_T}}^3 + 7.4210^{-6}\overline{R_{\theta_T}}^2 + 8.610^{-3}\overline{R_{\theta_T}} + 2.5625)\right] \tag{26}$$

$$R_{\theta_c} = \min\left[1.0; 1.62310^{-6}\,\overline{R_{\theta_T}}^{2} - 1.22810^{-3}\,\overline{R_{\theta_T}} + 0.849\right]\,\overline{R_{\theta_T}} \tag{27}$$

to be used with $\sigma_{\theta_T} = 10$. Another important element of the model is the Langtry correlation, which expresses the limit value of $\overline{R_{\theta_T}}$ before its advection into the boundary layer for comparison to a 'local' estimation of the physical boundary layer momentum thickness. This correlation, derived from the Abu-Ghannam & Shaw criterion, gives the transition value of R_{θ_T} as a function of a gradient parameter $F(\lambda_\theta)$, and is defined as :

$$\begin{cases} R_{\theta_T} = \left(1173.51 - 589.428\,Tu + \dfrac{0.2196}{Tu^2}\right) F(\lambda_\theta) \quad \text{if} \quad Tu \leq 1.3 \\ R_{\theta_T} = 331.5\,(Tu - 0.5658)^{-0.671}\,F(\lambda_\theta) \quad \text{if} \quad Tu > 1.3 \\ F(\lambda_\theta) = 1 - (-12.986\lambda_\theta - 123.66\lambda_\theta^2 - 405.689\lambda_\theta^3)\exp\left(-\left[\dfrac{Tu}{1.5}\right]^{1.5}\right) \text{ if } \lambda_\theta \leq 0 \\ F(\lambda_\theta) = 1 + 0.275\,[1 - \exp(-35.0\lambda_\theta)]\exp\left(\dfrac{-Tu}{0.5}\right) \quad \text{if} \quad \lambda_\theta > 0 \end{cases} \tag{28}$$

where $\lambda_\theta = \frac{\theta^2}{\nu}\frac{\mathrm{d}U}{\mathrm{d}s}$ represents the pressure gradient effect. This parameter is locally defined, it is different from the Pohlhausen parameter introduced before, which was function of the wall pressure or of the velocity at the boundary layer edge. The Langtry correlation applies for

$$0.03 \leq Tu \leq 9\%$$

$$-0.1 \leq \lambda_\theta \leq 0.1$$

$$R_{\theta_T} \geq 20$$

Figures 3 and 4 have pointed out the limitations of this empirical formulation when large pressure gradients or Mach numbers are at stakes.

Work was conducted at ONERA in order to extend this model to crossflow prediction, using the Kohama parameter. This parameter, introduced by Kohama & Davis [26], writes

$$C_K = R_\theta\sqrt{\frac{\theta}{r}} \tag{29}$$

It is similar to a Görtler number where the wall radius of curvature r is replaced by that of the streamline. It was confirmed during this study that a second transition criterion could be used in parallel to the first, and promising results were obtained in a first phase. The insertion into elsA did not produce so far acceptable results. At present, Menter's transition model is used mostly for bypass transition prediction on rotating surfaces and on turbine blades. Other extensions currently considered consist in extending the approach to other turbulence models, namely using $k-\omega$ Wilcox and $k-L$ Smith.

4 Examples of application

4.1 2D High Lift configuration

This 2D case is derived from the A310 geometry and were computed in the context of the French ALD (Aerodynamics at the limits of the flight envelope) project. The 'landing case' here considered in 2D is a quite difficult one as separation may rapidly result in unsteady flow. The mesh used extends to about 20 chords distance, with large mesh sizes at the limits of the domain. Hence the initialization of a turbulent kinetic energy level, requested for in the Menter transition approach, is unsatisfactory, the cells being too large for correctly transporting this information. In such case, two possible approaches are possible, one is to set the cut-off values of the model so that k and ω may not decay below the cut-off, the other being to impose the turbulence level (or k) at a short distance from the wing, which is coded in elsA. Present results were obtained with the second technique.

Computations were done with the two approches, AHD-GL for criterion, and Menter. Turbulent computation with Menter $k-\omega$ SST in elsA produces poor results in this case, so the turbulent curve is obtained here with the one equation Spalart model. Two results are shown with transition, the first one with transition criterion associated with Spalart, using a Jameson spatial scheme with a low dissipation parameter $ki4 = 0.008$. (In fact, $C_L(\alpha)$ curves are influenced by the values of $ki4$ when larger than 0.008. Below 0.008, results tend to become unsteady). The second result is obtained with the Menter transport equation model, used here with a second order Roe spatial scheme, with a Harten parameter of 0.01. The two results are quite close, showing that even for a natural transition case ($Tu = 0.15\%$), correct results may be obtained with both approaches, in 2D. Looking at the transition locations on the slat, figure 6 confirms that both AHD-GL and Menter predict similar results (in this case, $ki4$ was pushed to 0.004 for a small number of iterations). At this 23.2 deg. incidence, the orientation of the slat kink with the flow do not cause separation on either side in the leading edge region. Results in the figure compare turbulent to transitional results and seem to show that a small laminar region is predicted on both sides of the slat. Similar attempts in 3D did not produce comparable comparisons so far.

4.2 3D High Lift configuration

This section looks into the impact of natural transition on a 3D High Lift case, namely the KH3Y configuration which was selected during the EUROLIFT project [27], and consider the impact of transition location over a large range of Reynolds numbers. In the context of the European project ALEF, it was proposed to look at the Reynolds number impact on the CL_{max} evolution, to see if experimental results of figure 7 could be reproduced and explained.

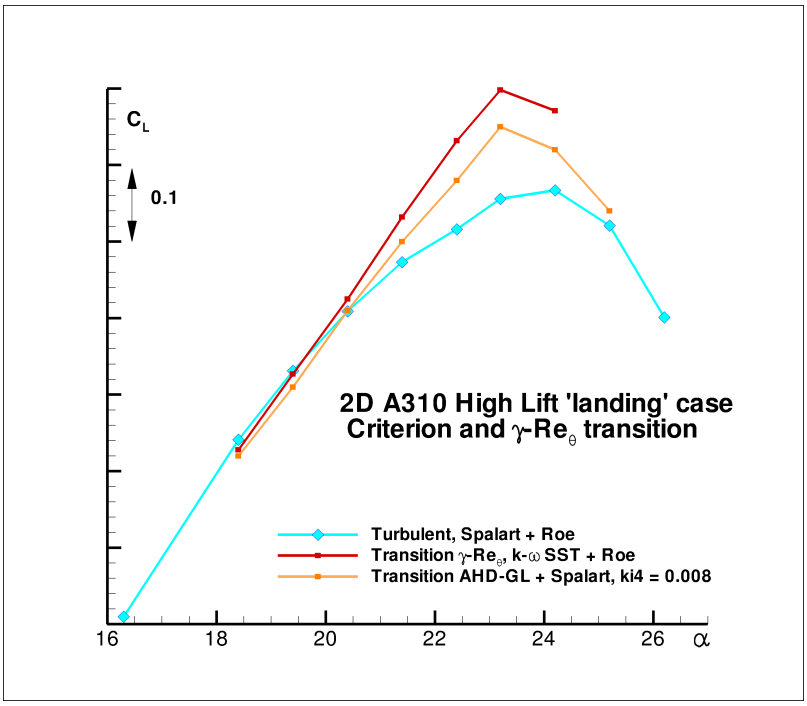

Figure 5: $C_L(\alpha)$ curves obtained with the two transition models

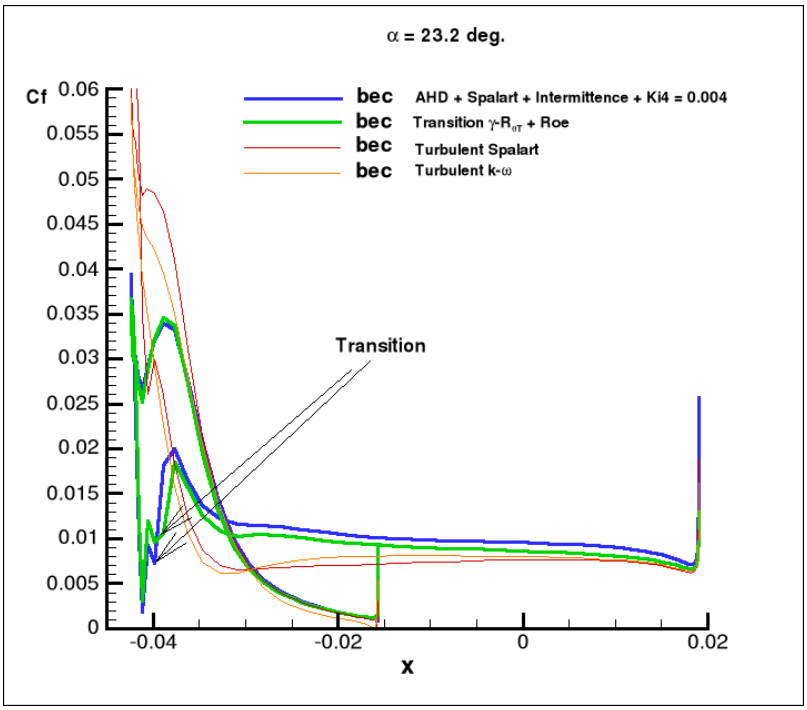

Figure 6: C_f distributions with transition (thick lines) compared to fully turbulent computations (thin lines)

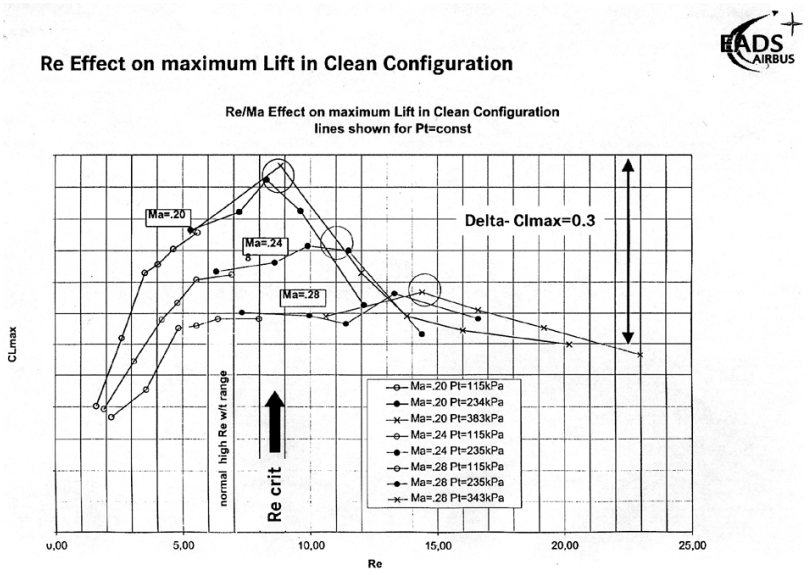

Figure 7: CL_{max} evolution with chord Reynolds number (Courtesy of Airbus)

In order to look at the Reynolds number impact, a refined mesh of 15 million nodes was produced at ONERA with a larger number of cells, around 50, within the boundary layer, and an increased number of sections along the windspan. Note that this mesh may be used for Reynolds numbers between about 4 and 15 10^6 with a laminar boundary layer, but that the boundary layer becomes too thick at lower Reynolds numbers, and its outer part is then not refined enough. In fully turbulent mode, the refined mesh can be used from 1 to 15 million without any problem. Transition computation were conducted using the classical Jameson scheme with $ki4 = 0.032$, and with the AHD-GL criteria coupled with C1 for transition prediction. The turbulence model is here the one equation Spalart-Allmaras.

Figure 8 shows the evolution of $CL(\alpha)$ for various Reynolds numbers computed in fully turbulent mode and with transition. In the first case, CL_{max} is seen to increase monotonically, while a different evolution is found with transition. In that case, CL_{max} increases up to $Re_C = 10^6$, then both CL_{max} and α_{max} decrease sharply. In these computations, transition is computed on the slat and the upper flap surfaces, while the main wing is assumed fully turbulent due to contamination.

Figure 9 shows a similar evolution as was observed on figure 7. Taking into account transition produces larger values of CL_{max} at low to medium Reynolds numbers, compared to fully turbulent computation, with a maximum value for a given value of the Reynolds number. Further increase in Reynolds number will result in a fully contaminated wing, with the CL_{max} curve rejoining the turbulent one. The prediction of such evolution is quite important when attempting to analyse low to medium Reynolds number wind tunnel tests and to extrapolate from these conditions to larger Reynolds number conditions.

Results presented so far did not take into account attachment line contamination (often

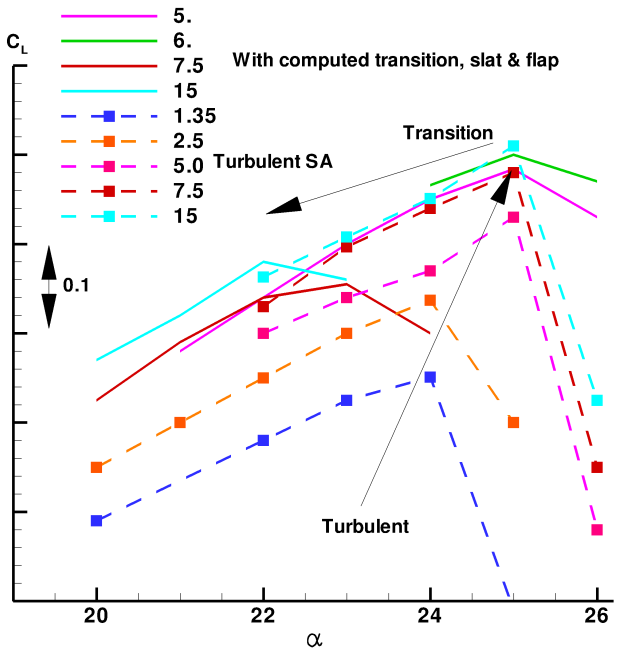

Figure 8: CL_α curves showing the effects of Reynolds number and transition prediction

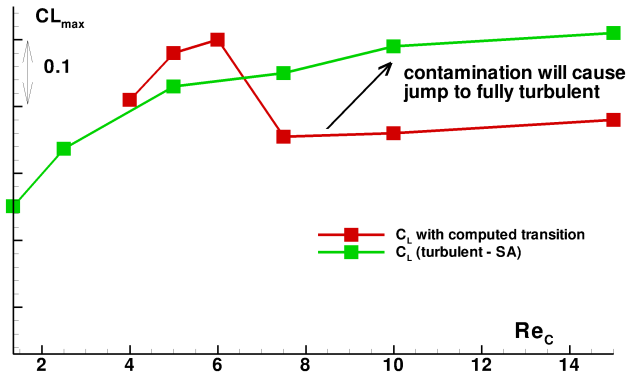

Figure 9: CL_{max} evolution with Reynolds number : impact of transition prediction

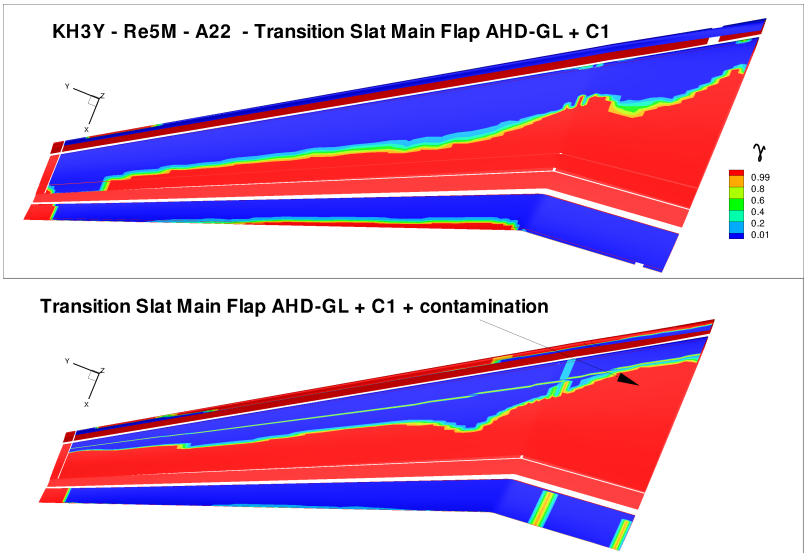

Figure 10: Example of contamination prediction for the KH3Y wing

referred to as Attachment Line Transition, ALT) The elsA code contains a model for contamination, which was tested with this case. From previous analysis, it was found that contamination will start over the main wing around $Re_C = 5\,10^6$, and will be observed on the slat around $8\,10^6$. Figure 10 indeed shows the impact on contamination on the main wing lower surface, where contamination is maintained as long as $\overline{R}$ remains above 250. In the present case, only part of the span is contaminated. It may be observed that only the lower surface is seen contaminated, while both upper and lower sides should be. This shows that the contamination criteria needs some improvement. With contamination included, figure 10 also shows some differences over the slat. Careful examination reveals that contamination does not occur on the slat at $5\,10^6$, but that the transition line is shifted with a larger turbulent zone in the second case. Attempts at treating this configuration using the Menter transition model did not generate significant results. Crossflow instabilities play a major role in this case, which is not accounted for in that approach.

4.3 Case of a laminar low-sweep wing

This case is presented to show the limits of the C1 crossflow criterion applied to a transonic, laminar low sweep wing. Results shown were computed both with elsA and with the 3D boundary layer code 3C3D. In case of elsA, C1 predicted a fully laminar flow, from wing root to tip, and from the leading edge to the shock, a result that needed to be confirmed. Computations done with 3C3D, shown on the figure, confirm that C1 does not predict transition here, because the crossflow displacement thickness Reynolds number $R_{\delta 2}$ remains too small, below 120. On the contrary, using the 3D Parabola code (a simplified stability method) inside 3C3D, a turbulent region is predicted in the inner wing region. These results were also confirmed by exact stability calculation. They show that C1, based mostly on the values of R_{δ_2} should be used with care in case of laminar wings. Crossflow stability is determined by the velocity profile, and has been shown to be

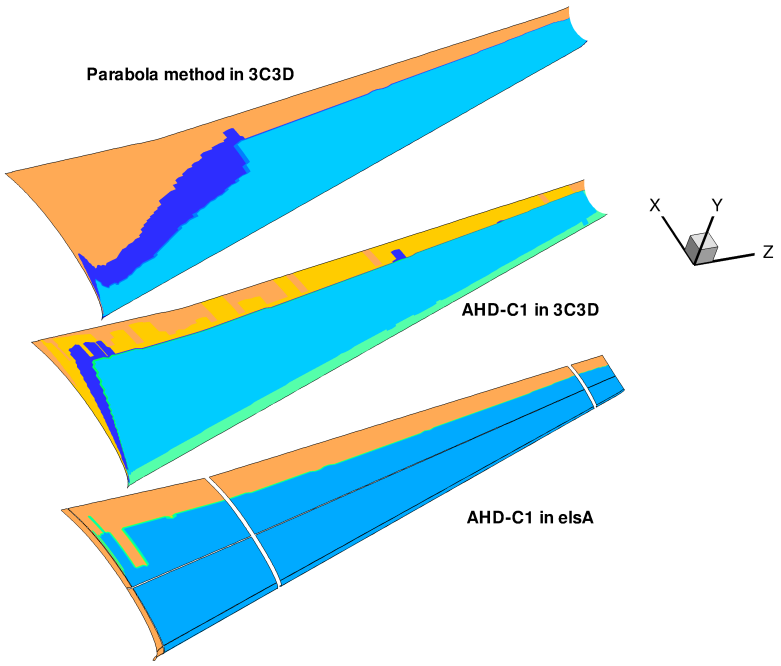

Figure 11: Comparison of several approaches for crossflow transition on a laminar swept wing

function of the characteristics of the profile inflection point. The C1 criterion is usually fine when dealing with classical wings, for which crossflow transition may appear in the first 10% chord.

5 Recent evolutions

The AHD criterion has been extended to higher Mach numbers on adiabatic walls. In the present version of elsA, there are two variants of AHD, one up to Mach 1.6 dealing with hot walls ($T_w/T_f \geq 1/$), and a second up to Mach 4 but restricted so far to adiabatic walls. This new extension was developped in the context of the Garteur AG51 project. Figure 12 shows comparisons of results in elsA and 3C3D, obtained for three values of the turbulence level. The two models, AHD16 and AHD4 (the first being the extension to Mach 1.6, the second to Mach 4, are compared in both codes. Continuous and dotted lines were obtained in 3C3D, with five levels of pressure gradients. The middle curve correspond to zero gradient. elsA's results were obtained here only for flat plate flows, and results are given with AHD4 up to Mach 4.5. Only the first mode is represented in the model. The limit between modes 1 and 2 is function of the pressure gradient, mode 1 remains the most amplified up to Mach 4, and to Mach 4.5 in zero pressure gradient. A separate model dealing with second mode instabilities would be necessary in order to consider higher Mach number flows

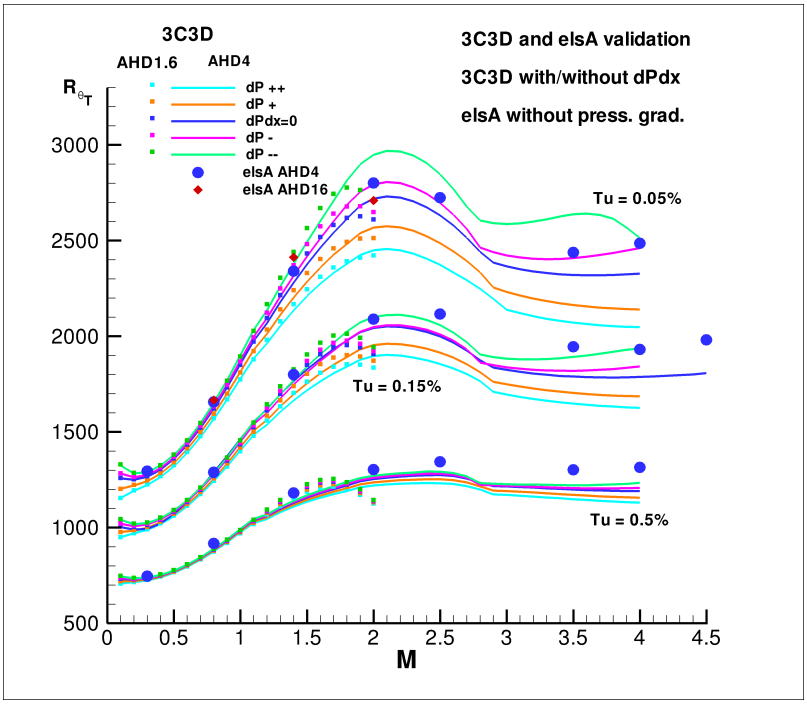

Figure 12: Results obtained with the extended AHD criterion, in elsA and 3C3D

6 Conclusion

The elsA software is quite well equiped with transition prediction tools, allowing to consider both general aviation problems, high speed vehicles, and contribute to the design of future laminar wings. Applications related to rotating surfaces were not presented here, but are also of interest. In parallel evaluation of the two available approaches, transition criterion versus the Menter approach, have been presented with a focus on natural transition of attached flows. While Menter seems better adapted for bypass type transition, it may also be applied for 2D low turbulence cases. Extension to full 3D remain unsatisfying, in part due to the limitation of its transition criterion. Present implementation of transition lines in elsA is not compatible with the Chimera approach, and is considered cumbersome for complex configurations. Nevertheless, criteria are quite precise and allow rapid estimation of the transition lines (some 3000 iterations in multigrid approach starting from uniform flow). Still, the evolution towards more and more complex configurations call for a simplified user interface, which should appear with the replacement of the transition lines with the use of transport equations.

Improvements are expected with regard to the treatment of contamination and relaminarization.

Another domain in which progresses are expected is the modelling of the transition region itself, which may need to be adapted for the turbulence model used, and the modelling of transition in laminar separation bubbles, with the need to predict the appearance of short or long bubbles.

Aknowledgements

Results presented here were obtained in the context of the European project ALEF, and in Research projects ANANAS and ALD, supported by the French DGAC and Dassault Aviation. Compressible extension of AHD is here developped in the frame of the GARTEUR AG51 project.

REFERENCES

[1] **M. Morkovin**. On the many faces of transition. In C. Wells (éd.), *Viscous Drag Reduction*. Plenum, 1969.

[2] **D. Arnal**. Three-dimensional boundary layers: Laminar-turbulent transition. In *Computation of Three-dimensional Boundary Layers Including Separation*, AGARD Rep 741. AGARD-FDP-VKI Special Course, April 1986.

[3] **D. Arnal**. Boundary Layer Transition: Prediction, Application to Drag Reduction. In *Skin Friction Drag Reduction*, AGARD Rep 782. AGARD-FDP-VKI Special Course, March 1992.

[4] **D. Arnal**. Boundary Layer Transition: Predictions based on linear Theory. In *Progress in Transition Modelling*, AGARD Rep 793. AGARD-FDP-VKI Special Course, Madrid et Bruxelles, March-April 1993.

[5] **L. Cambier, S. Heib & S. Plot**. The Onera elsA CFD software: input from research and feedback from industry. *Mechanics & Industry*, **14** (3), 159–174, Jan. 2013.

[6] **L. Cambier & M. Gazaix**. elsA : an efficient object-oriented solution to CFD complexity. AIAA Paper 2002-0108, 2002.

[7] **D. Arnal, G. Casalis & R. Houdeville**. Practical Transition Prediction Methods: Subsonic and Transonic Flows. In *Advances in Laminar-Turbulent Transition Modelling*, RTO-AVT 151. RTO-AVT-VKI Special course, 2008.

[8] **D. Arnal, H. Habiballah & E. Coustols**. Théorie de l'instabilité laminaire et critères de transition en écoulement bi et tridimensionnel. *La Recherche Aérospatiale*, **1984-2**, 1984.

[9] **E. Coustols**. *Stabilité et transition en écoulement tridimensionnel : cas des ailes en flèche*. Ph.D. thesis, ENSAE, June 1983.

[10] **D. Arnal, E. Coustols & J. Juillen**. Etude expérimentale et théorique de la transition sur une aile en flèche infinie. *La Recherche Aérospatiale*, **1984-4**, 1984.

[11] **C. Gleyzes, J. Cousteix & J. Bonnet**. Theoretical and Experimental study of Low Reynolds Number Transitional Separation Bubbles. In *Proceeding of the conference on low Reynolds number airfoil aerodynamics, UNDAS-CP-77B123, University of Notre Dame, Indiana*, June 1985.

[12] **F. Menter, R. Langtry, S. Likki, Y. Suzen, P. Huang & S. Völker**. A Correlation-based Transition Model using Local Variables Part I - Model Formulation. In *ASME GT2004-53452*. ASME Turbo Expo 2004 Power for Land, See and Air, Vienna, Austria, 14-17 June 2004.

[13] **F. Menter, T.Esch & S.Kubacki**. Transition Modelling Based on Local Variables. In *ETMM 5*. 5^{th} International Symposium on Engineering Turbulence Modelling and Measurements, Mallorca, Spain, 2002.

[14] **R. B. Langtry**. *A Correlation-Based Transition Model Using Local Variables for Unstructured Parallelized CFD Codes*. Ph.D. thesis, Stuttgart University, May 2006.

[15] **C. Content**. *Méthode innovante pour le calcul de la transition laminaire-turbulent dens les codes Navier-Stockes*. Ph.D. thesis, Institut Supérieur de l'Aéronautique et de l'Espace, May 2011.

[16] **A. Benyahia**. *Mise en Oeuvre et Evaluation d'un Modèle de Transition à Equations de Transport pour la simulation d'écoulements en Turbomachines*. Ph.D. thesis, Université Toulouse III, Ecole Doctorale MEGEP, Dec. 2012.

[17] **J. Perraud, D. Arnal, G. Casalis, J. Archambaud & R. Donelli**. Automatic transition predictions using simplified methods. *AIAA Journal*, **47** (11), 2676–2684, Nov. 2009.

[18] **J. Dunham**. Prediction of Boundary Layer Transition on Turbomachinery Blades. AGARD Meeting Boundary Layer in Turbomachines, Paris, 1972.

[19] **N. J. Seyb**. The Role of Boundary Layers in Axial Flow Turbomachines and the Prediction of their Effects. Rolls-Royce Limited, Bristol, Engine Division, 1971.

[20] **B. Abu-Ghannam & R. Shaw**. Natural Transition of Boundary Layer - The Effect of Turbulence Pressure Gradient, And Flow History. *Journal of Mechanical Engineering Science*, **22** (5), 213–228, 1980.

[21] **M. Drela & M. B. Giles**. Viscous-Inviscid Analysis of Transonic and Low Reynolds Number Airfoils. *AIAA Journal*, **25** (10), 1347–1355, 1987.

[22] **R. E. Mayle**. The Role of Laminar-Turbulent Transition in Gas Turbine Engines. *ASME J. of Turbomachinery*, **113**, 509–537, 1991.

[23] **D. Arnal, R. Houdeville, A. Séraudie & O. Vermeersch**. Overview of laminar-turbulent transition investigations at ONERA Toulouse. AIAA Paper 2011-3074, 41st AIAA Fluid Dynamics Conference and Exhibit, June 2011.

[24] **J. Cliquet**. *Calcul de la transition laminaire-turbulent dans les codes Navier-Stokes. Applications aux géométries complexes.* Ph.D. thesis, SUPAERO, Oct. 2007.

[25] **E. R. van Driest & C. B. Blumer**. Boundary Layer Transition : Free-stream Turbulence and Pressure Gradient Effects. *AIAA Journal*, **1** (6), 1303–1306, 1963.

[26] **Y. Kohama & S. Davis**. A new parameter for predicting crossflow instability. *JSME international Journal Série B, Fluids and thermal engineering*, **36-B(1)**, 80–85, 1993.

[27] **F. Moens, J. Perraud, P. Iannelli, T. Toulorge, P. Eliasson & A. Krumbein**. Transition prediction and impact on 3D high lift wing configuration. AIAA Paper 2007-4302, June 2007.